Cell Reports
Physical Science

CellPress
OPEN ACCESS

Article

Radiative cooling and thermoregulation in the earth's glow

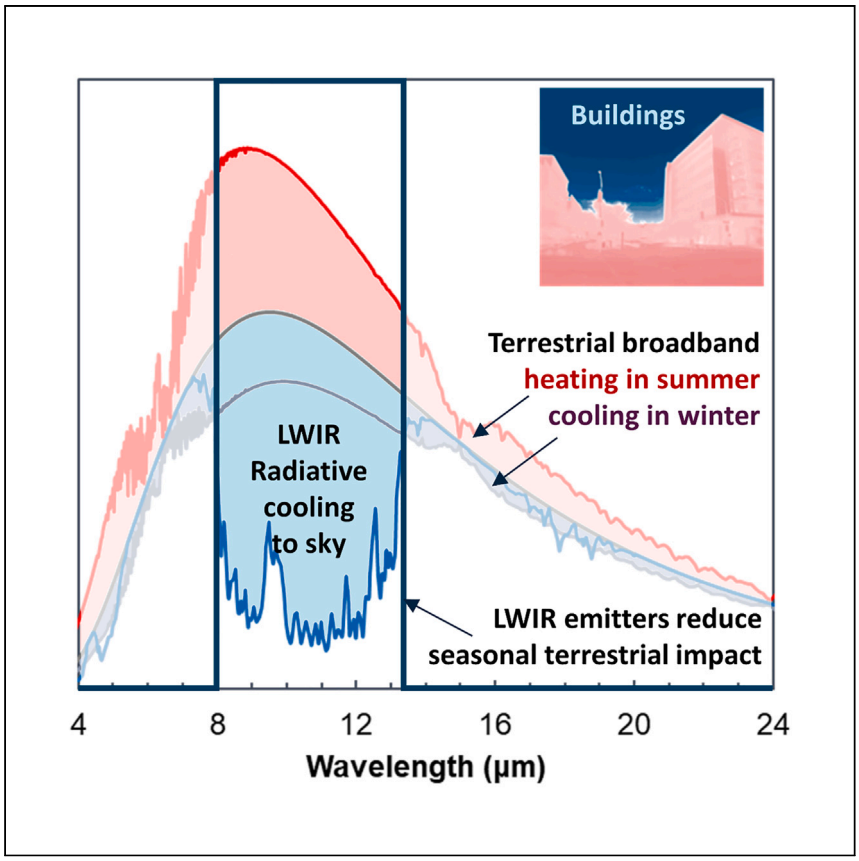

Mandal et al. propose and demonstrate that selective longwave infrared-emissive exterior envelopes can keep walls and windows of buildings cooler than traditional exterior envelopes in hot weather and warmer in cold weather. Achievable by simple means, this passive radiative thermoregulation can enable untapped energy savings in buildings.

Jyotirmoy Mandal, Jyothis Anand, Sagar Mandal, John Brewer, Arvind Ramachandran, Aaswath P. Raman

jm3136@princeton.edu (J.M.)
aaswath@ucla.edu (A.P.R.)

Highlights

A novel, passive radiative thermoregulation mechanism for walls and windows

Buildings lose narrowband heat to the sky but exchange broadband heat with the earth

Vertical LWIR emitters stay cooler than broadband ones in hot weather and warmer in cold

Thermoregulation by this simple and static design yields untapped energy savings

Mandal et al., Cell Reports Physical Science 5, 102065
July 17, 2024
https://doi.org/10.1016/j.xcrp.2024.102065

Cell Reports
Physical Science

CellPress
OPEN ACCESS

Article

Radiative cooling and thermoregulation in the earth's glow

Jyotirmoy Mandal,[1,2,6,8,*] Jyothis Anand,[3] Sagar Mandal,[5] John Brewer,[2] Arvind Ramachandran,[4] and Aaswath P. Raman[2,7,*]

SUMMARY

Efficient passive radiative cooling of buildings requires an unimpeded view of the sky. However, vertical facades of buildings mostly see terrestrial features that become broadband-radiative heat sources in the summer and heat sinks in the winter. The resulting summertime terrestrial heat gain by buildings negates or overwhelms their narrowband longwave infrared (LWIR) radiative cooling to space, while the wintertime terrestrial heat loss causes overcooling. We show that selective LWIR emitters on vertical building facades can exploit the differential transmittance of the atmosphere toward the sky and between terrestrial objects to achieve higher summertime cooling and wintertime heating than conventionally used broadband emitters. The impact of this novel and passive thermoregulation is comparable to that of painting dark roofs white and is achievable with both novel and commonplace materials. Our findings represent new and remarkable opportunities for materials design and untapped thermoregulation of entities ranging from buildings to human bodies.

INTRODUCTION

With global increases in temperatures posing fundamental economic, health, and security risks to human civilization, maintaining habitable built environments has become one of the most important challenges of our times. Cooling and heating buildings currently consumes 12% of energy globally, with energy use for cooling in particular expected to grow dramatically by 2050.[1] Unfortunately, prevalent thermal management methods, such as air conditioners (ACs) and heaters consume large amounts of electricity and fuel, generate their own heat, and cause direct and indirect greenhouse gas emissions. Furthermore, in urban areas, the net heat from AC units and the prevalence of human-made structures that trap solar heat and inhibit evaporative cooling all lead to exacerbated local heating. Indeed, active thermoregulation methods may exacerbate climate change[2] and the resulting cooling needs.[3–5] Therefore, they are not sustainable solutions for large-scale heat management in built environments.

A central mechanism to reduce the need for active cooling and heating is the control of radiative heat flows into and out of buildings. To this end, decades of research have explored strategies to control solar heat gain through different components of the building envelope (e.g., roofs, walls, and windows). Innovations in materials and optical design have enabled tailored responses to different bands of the solar spectrum (UV, visible, and near-infrared wavelengths). However, the built environment also radiatively emits and absorbs heat from its immediate environment over

[1]Department of Civil & Environmental Engineering, Princeton University, Princeton, NJ 08540, USA

[2]Department of Materials Science and Engineering, University of California, Los Angeles, Los Angeles, CA 90025, USA

[3]Buildings and Transportation Science Division, Oak Ridge National Lab, Oak Ridge, TN 37831, USA

[4]Arizona State University, Tempe, AZ 85281, USA

[5]Seattle, WA 98115, USA

[6]X (formerly Twitter): @Jyoti299792458

[7]X (formerly Twitter): @aaraman

[8]Lead contact

*Correspondence: jm3136@princeton.edu (J.M.), aaswath@ucla.edu (A.P.R.)

https://doi.org/10.1016/j.xcrp.2024.102065

the thermal infrared (TIR) wavelengths (λ ~2.5–40 μm). This ubiquitous heat exchange has, in large part, not been leveraged to enhance efficiency in buildings.

One important exception has been the radiative cooling of sky-facing building facades, which involves the radiation of heat through the long-wavelength-infrared (LWIR; λ ~8–13 μm) atmospheric transmission window into outer space. Because the earth is at a higher temperature (~290 K) than outer space (~3 K), the radiative heat loss can be large if a sky-facing surface has a high emittance (ϵ) in the LWIR wavelengths (ϵ_{LWIR}).[6] If it also has a sufficiently high solar reflectance (R_{solar}), it can lose heat and radiatively cool to sub-ambient temperatures even under sunlight.[6] The fundamentally passive nature and net cooling effect of radiative cooling make it a sustainable alternative to active cooling systems. Research on the topic has yielded a range of sky-facing designs, such as traditional white paints,[7–9] porous polymers,[6,10] silver-backed multilayer films,[11] polymers,[12–14] dielectrics,[15–17] and polymer-dielectric composites.[12,18–21] These designs encompass both selective LWIR emitters, which can achieve deep sub-ambient temperatures, and broadband thermal emitters, which are suitable for operation at or near ambient temperatures. Other works have also identified strategies to tune radiative cooling to different weather and climate conditions.[22–24]

While radiative cooling has been well studied for horizontal, sky-facing surfaces, most of the surface area of a typical building may be vertically oriented. Controlling the temperature of vertical facades is far more challenging, since they see not only the cold sky, but also the terrestrial environment, which becomes warm during the summer and cold during the winter. The thermal glow from terrestrial features can drastically reduce, or even reverse, radiative cooling in the summer, while its reversal can cause overcooling in the winter. To our knowledge, the impact of seasonally varying terrestrial irradiance on vertical surfaces has not been considered in prior works.[25–28] Therefore, identifying a mechanism to passively thermoregulate vertical facades that see the earth's glow remains an important, unaddressed challenge.

In this report, we demonstrate that scalable, selective LWIR-emissive materials can achieve passive and seasonal radiative thermoregulation when vertically oriented and hold the potential for substantial, untapped energy savings in buildings. To our knowledge, this is a novel phenomenon that we report for the first time. Our approach is based on the differential transmittance of the atmosphere toward the sky (narrowband, LWIR) and between terrestrial objects (broadband), which makes buildings susceptible to seasonal terrestrial heat flows. Our proposed solution, selective LWIR emitters, reflect large bandwidths of broadband radiative heat flows to and from the earth when vertically oriented, even as they radiate and lose LWIR heat into the sky. Consequently, compared to broadband emitters, they can yield considerably greater cooling in the summer and heating in the winter. This is significant for buildings, as traditional construction materials,[29] white paints[6,8,29] and composites,[19] are broadband emitters. Furthermore, in optimizing seasonal radiative heat flows with a *static* design, our approach represents a fundamentally different, subtler, and yet easily achievable thermoregulation than those of adaptive or dynamic designs.

We first develop a theoretical model and show that standard cooling potentials show that, relative to vertical broadband emitters, LWIR emitters achieve summertime cooling of up to ~50 W m^{-2} and wintertime heating of ~15 W m^{-2}. The values are similar in magnitude to absolute cooling potentials of sky-facing designs.[6,11,19] This is validated by proof-of-concept experiments, which show that vertically

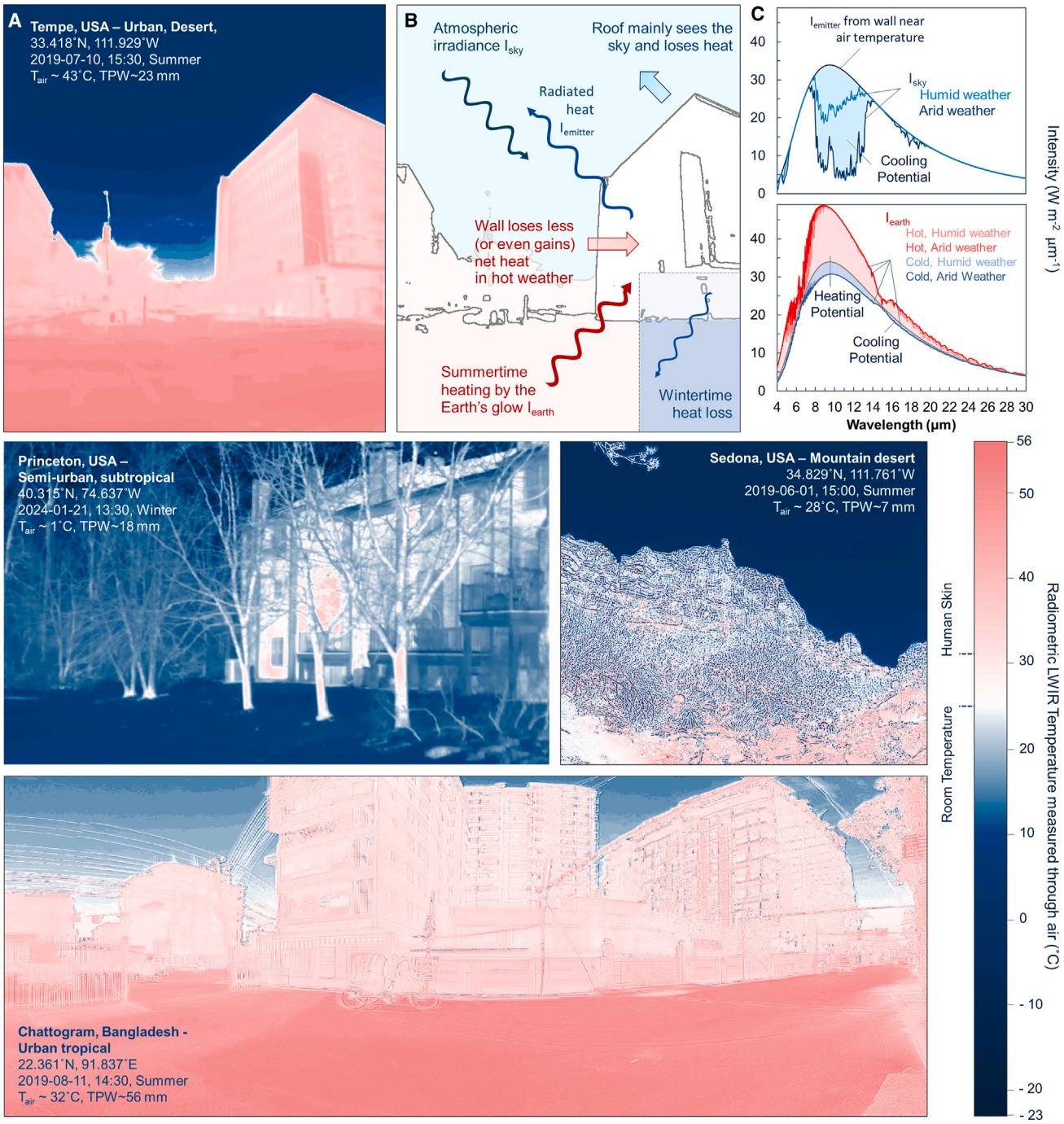

Figure 1. The seasonal thermal environment observed by vertical building facades

(A) Panoramic LWIR thermographs of locations in Tempe, Princeton, and Sedona in the United States and Chattogram in Bangladesh, representing rural and urban locations in different climate zones from the vantage point of a vertical wall. Further examples are shown in Figures S1 and S13. The color bar represents effective radiative temperatures assuming $\epsilon = 1$ for the environment (Note S1). During the summer in Tempe, Sedona, and Chattogram, the ground and other terrestrial features become considerably warm radiators during the day, while the sky, depending on the total precipitable water (TPW) in the atmosphere, exhibits varyingly cold LWIR temperatures. Thus, during summer days, terrestrial features may warm objects like walls and humans in their view. In the winter, the terrestrial environment becomes a cold heat sink for buildings, as shown in the thermograph for Princeton. Figures S1 and S13 show more such environments.

(B) Schematic showing the radiative heat transfer between a vertical wall and the ground and sky in its view.

Figure 1. *Continued*

(C) The radiated power ($I_{emitter}$) from a perfect broadband emitter at the ambient temperature 32°C and hemispherical irradiances from the ground (I_{earth}, at radiative temperatures 55°C (hot) and 26°C (cold), and the sky (I_{sky}) as seen through the atmosphere (Figure S3). Cases for two different humidities (low and very high TPW values of 10.5 and 58.6 mm, respectively) are shown. Shaded areas show the possible heat loss to the sky (blue) and gain/loss to the ground (red/blue) under full view.

oriented selective LWIR emitters completely exposed to the weather stay ~0.43°C–0.86°C cooler than broadband emitters in the summer and 0°C–0.21°C warmer during the winter. The large differential heat flows for buildings, which these temperature differences represent, are demonstrated with power flow experiments, which show ~21 W m^{-2} relative cooling and ~10–30 W m^{-2} relative heating by selective LWIR emitters in hot and cold terrestrial environments, respectively. Building-level energy simulations show that using our approach on walls and windows can lead to substantial energy savings, equivalent to US$$10^1$–$10^3$/year in cost and 1–10 tons/year in CO_2 emissions. This is comparable to or greater than savings achievable by painting dark roofs white. Crucially, this approach is *complementary*, and not an alternative, to the benefits of high solar reflectance on roofs and walls. Our analysis also shows that this thermoregulation persists for dark-to-highly solar-reflective ($R_{solar} \gtrsim 0.50$) vertical facades that are directly sunlit and even darker solar-reflective facades that are diffusely lit ($R_{solar} \lesssim 0.40$). Furthermore, in hot and congested urban environments with a narrow view of the sky, the cooling effect is heightened.

Motivated by the possibilities, we explored both novel and known LWIR emitters, like metallized polypropene (PP), paint resins, and ceramics, which have the selective ϵ_{LWIR} needed to outperform conventional broadband emitters and whose scalability, costs, and compatibility with buildings could see them quickly implemented, especially in resource-poor settings where the need for thermoregulation is most acute. These results, which are founded on a new insight into the interplay of atmospheric optics and seasonality of the radiant environment, highlight a remarkable opportunity for radiative thermoregulation of built environments worldwide: immediate and untapped gains in building energy efficiency, achievable by replacing conventional vertical building envelopes with selective LWIR emitters.

RESULTS AND DISCUSSION

Theoretical model

Research on radiative cooling typically assumes a scenario where a horizontal radiative cooler radiates heat to an unobstructed view of the sky. However, this assumption neglects a large fraction of the surface area for radiative heat transfer in buildings: walls and other vertical facades. Walls have at least half of their field of view subtended by terrestrial features. The panoramic thermographs in Figures 1A and S1 represent examples of different landscapes and weathers across the world. The presence of terrestrial objects in the field of view has two effects. First, it reduces the spatial window for heat loss into the sky. Second, terrestrial objects themselves radiate significant amounts of heat, especially under the summertime sun (e.g., >60°C for dry, non-vegetated surfaces).[30,31] Effectively, this replaces the heat sink of the sky with heat sources. Consequently, the cooling potential ($P_{cooling}$) of a vertical surface, usually defined as the difference between the radiated power from the surface ($I_{emitter}$) at ambient temperature and the downwelling hemispherical atmospheric irradiance (I_{sky}) (Figure 1B), now takes the form:

$$P_{cooling} = I_{emitter} - I'_{sky} - I'_{earth} \sim I_{emiter} - vI_{sky} - (1 - v)I_{earth}. \quad \text{(Equation 1)}$$

Here, I'_{sky} and I'_{earth} represent the sky and terrestrial irradiances on the surface, I_{earth} represents the "earth glow" or hemispherical irradiance from the earth (Figure 1B),

and the sky view factor v is $\lesssim$0.5. A detailed version is provided in Note S3. The problem is further compounded by the semi-transmissive atmosphere, which is thick (>20 km) along skyward directions between buildings and space and thus appreciably transparent only in the LWIR wavelengths, but much thinner ($\sim 10^0$–10^2 m) and thus transparent across the thermal infrared wavelengths between buildings and their environment (Figure S3). As a result of this atmospheric bias, radiative heat loss to outer space occurs mainly in the narrow LWIR band (λ ~8–13 μm) (Figures 1B and 1C, top), but radiative heat gain from terrestrial sources is broadband (λ ~2.5–40 μm) (Figures 1B and 1C, bottom), i.e., both inside and outside the LWIR band.

The effect of these heat flows on the summertime cooling performance of broadband-emissive radiative coolers like paint coatings can be significant. As shown in Figure 1C, since radiated heat scales as T^4, even moderately above-ambient terrestrial heat sources can have a broadband heating potential that counters or outweighs the narrowband LWIR cooling potential of the sky, especially when it is humid. This is observed in the above-ambient pyrgeometric temperatures of the thermal environment as seen by vertical facades in warm locations (Note S2; Table S1). Given that vertical facades have broadband-emissive[32–34] terrestrial objects in the field of view, and have building envelopes that are broadband thermal emitters/absorbers,[19,29] broadband heat radiated from terrestrial features can greatly reduce, or even reverse, radiative cooling in the summer.

In the winter, the radiative environment changes: long nights and weak sunlight mean that the ground is often at sub-ambient temperatures due to radiative cooling[29] and acts as a broadband heat sink (Figures 1A, Princeton, and 1C). Thus, broadband-emissive building envelopes experience undesirable heat gain in the summer and loss in the winter (Figure 1B).

Our solution to the undesirable heat flows experienced by vertical surfaces arises from the differential atmospheric transmittance that allows narrowband LWIR heat loss to the sky and broadband terrestrial summertime heat gain and wintertime loss. We propose that radiative coolers that selectively emit and absorb radiation in the LWIR atmospheric window, and reflect other thermal wavelengths, can optimally harness this phenomenon to enable improvements in the net heat flows into and out of buildings. To illustrate this capability, we choose the case of a vertical surface similar to that in Figure 1B, which has equal views of the cold sky and a hot ground (Figure S2). As shown in Figure 2A, broadband emitters like traditional building envelopes absorb and emit thermal radiation both within and outside the LWIR window. Consequently, for a perfect broadband emitter (Figure S4), the skyward LWIR radiative heat loss (blue shaded area) is negated or outweighed by the summertime terrestrial radiative heat gain (darker and lighter red shaded areas), leading to heating. However, if heat is gained or lost only in the LWIR window and reflected elsewhere, broadband heat gain can be minimized (to the darker red shaded area) without reducing LWIR heat loss to space, resulting in a large relative cooling compared to those achievable by broadband-emissive radiative coolers.

In the winter, the broadband emitter loses LWIR heat to the sky and broadband heat to the ground (green shaded area) (Figure 2B). In this scenario, the selective emitter reduces broadband terrestrial heat loss, enabling a relative heating effect. The selective emitter, therefore, achieves a passive radiative thermoregulation, arising purely from the atmosphere's spectral transmittance and seasonal variation in terrestrial irradiance.

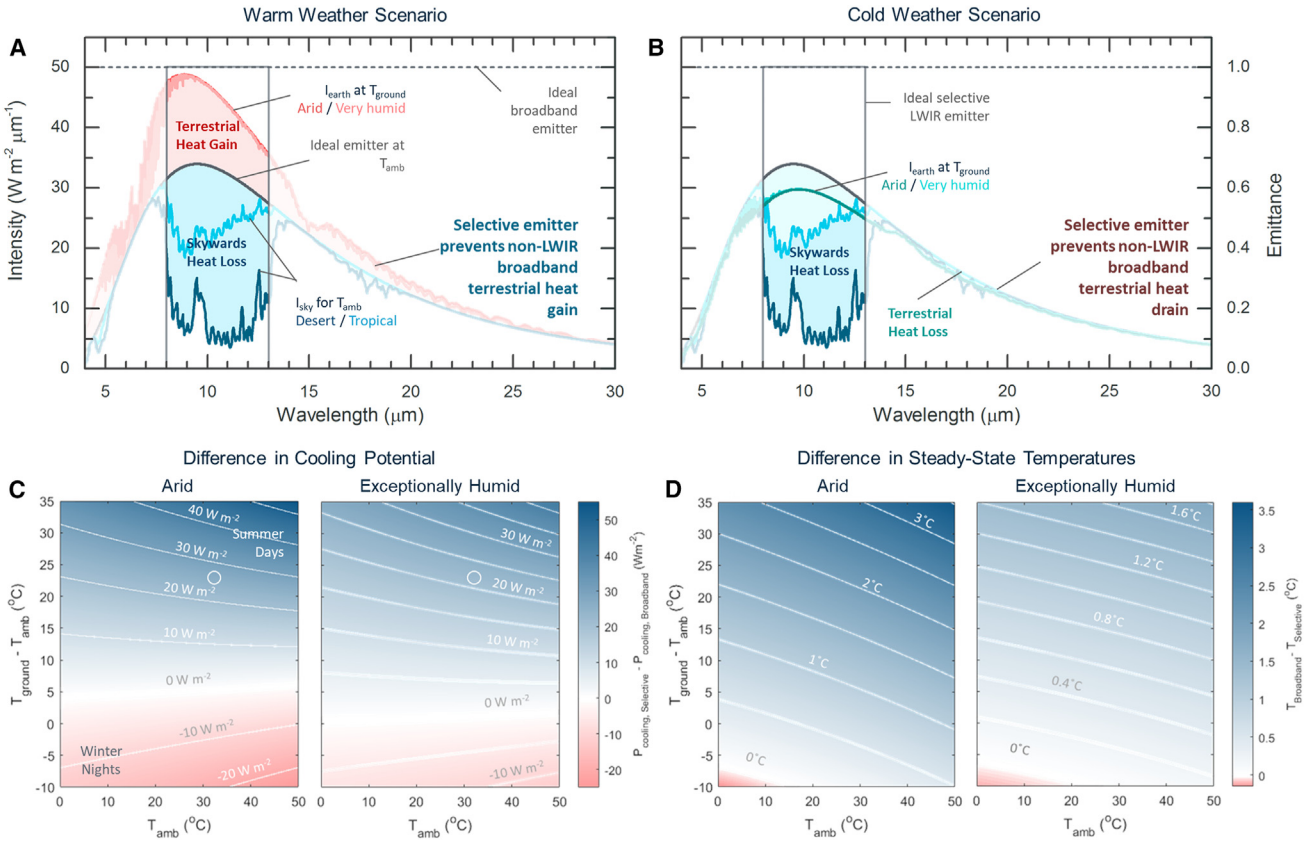

Figure 2. Physical mechanism of thermoregulation by selective LWIR emitters relative to broadband emitters

(A) The maximum possible heat gain (red) from the ground (T_{ground} ~55°C) and heat loss (blue) to the sky during a summer day, as shown for ideal broadband and selective emitters (Figure S4) at ambient temperature (T_{amb} ~32°C) under desert (TPW 10.5 mm) and exceptionally humid tropical (TPW 58.6 mm) climates. Note that the irradiances I_{sky} and I_{earth} are hemispherical values. For a vertical emitter with equal views of the sky and the earth, the red and blue areas are weighted by ½ to get I'_{sky} and I'_{earth}, and the difference represents the net cooling potential. By reflecting thermal radiation outside the window, the selective emitter filters out much of the broadband thermal radiation from the ground and enables greater cooling when the ground in view is hot.

(B) Analogous scenario for a winter night (T_{ground} ~8°C below T_{amb}), where the selective emitter prevents broadband radiative heat loss to the ground, leading to a seasonal thermoregulation capability.

(C) Differences between $P_{cooling}$ of an ideal selective LWIR emitter and a broadband emitter as a function of T_{ground} and T_{amb}. Values corresponding to the data in (A) are represented by open circles. Individual cooling potentials of the two emitters are presented in Figure S5.

(D) Analogous differences between steady-state temperatures of an ideal selective LWIR emitter and a broadband emitter assuming zero conductive heat flows and gentle winds. Individual steady-state temperatures of the two emitters are presented in Figure S6. It is clear from (C) and (D) that a selective LWIR emitter has a large relative cooling effect during hot weather and relative heating effect in cold weather—signifying a passive seasonal thermoregulation capability. For terrestrial-view factors >0.5, the cooling potential is heightened (Note S3; Figure S10). Cooling potential and steady-state temperature differences for two non-ideal emitters (Figure S7) are shown in Figures S8 and S9.

The cooling/heating potential of a vertical surface (Equation 1) depends on several factors, such as temperature of the emitter ($T_{emitter}$), the ambient air (T_{amb}), and the ground (T_{ground}); meteorological variables; view factors of objects in the environment; and conductive and convective coefficients (h) of materials. Together, these determine $I_{emitter}$, I_{sky}, I_{earth}, their view, and non-radiative heat flows. In this study, we choose the illustrative case of a vertical surface with equal views of the ground and the sky (i.e., v = 0.5) (Note S3), which corresponds to the minimum view factor of the terrestrial environment for a vertical surface. Compared to higher terrestrial view factors such as in congested cities, v = 0.5 is a conservative choice (Note S3). Calculations of theoretical cooling potentials and steady-state temperatures assuming negligible conductive heat flow show that a selective LWIR emitter can

have considerable benefits. As shown in Figure 2C, a selective LWIR emitter achieves a significantly greater $P_{cooling}$ than a broadband emitter when T_{ground} is considerably greater than T_{amb}, as might occur on sunny summer days. In deserts, where lower total precipitable water (TPW) levels enable greater LWIR heat loss into the sky, relative $P_{cooling}$ can exceed 50 W m^{-2}, which is comparable to the absolute $P_{cooling}$ of white paints.[29] A similar cooling effect occurs even in exceptionally humid conditions. Furthermore, in hot and congested urban environments ($v \sim 0.2$–0.3), the relative cooling increases by >10 W m^{-2} (Note S3). Conversely, when $T_{ground} < T_{amb}$, as is typical for winters or cold nights, a selective emitter shows a relative $P_{cooling}$ of ~ -15 W m^{-2}, i.e., a lowered heat loss. We note here that the values calculated here are for emitters held at T_{amb}. For building facades, which can be cooler than T_{amb} in the summer and warmer in the winter (Figure 1A; Note S5), these values would be greater.

A similar trend is seen in the differences in steady-state temperatures (Figure 2D). Under mild winds ($h \sim 10$ W m^{-2} K^{-1}), a selective LWIR emitter stays ~3°C cooler when the ground is hotter and at negligibly different temperatures from that of the broadband emitters when the ground is colder than the ambient air.

It should be noted that the results in Figure 2 are calculated independent of solar heat gain, i.e., assuming an R_{solar} of 1, or 0 solar absorption. Additional analysis shows that the relative summertime cooling by selective LWIR emitters over broadband emitters persists for solar heat gains as high as 50–100 W m^{-2} (Note S7). This is because the large difference in the ambient thermal irradiance ($vI_{sky} + (1 - v)\, I_{earth}$) absorbed by selective and broadband emitters is not easily overwhelmed by sunlight. Indeed, surfaces with $R_{solar} \gtrsim 0.90$ can achieve thermoregulation even when directly sunlit. When solar illumination over 24 h is considered, we find $R_{solar} \gtrsim 0.50$ to be sufficient for surfaces that see direct sunlight and much lower for surfaces that are diffusely lit (Note S7). Crucially, drops in summertime cooling due to sunlight are often offset by enhanced wintertime heating, meaning that the overall benefits are quite robust under solar absorption.

Verifying the phenomenon: Steady-state temperature measurements

To verify the theoretical results with proofs of concept, we performed a series of experiments where we exposed vertically oriented selective and broadband thermal emitters to summer and wintertime environments in Los Angeles and Princeton (Figures 3 and 4). A 508-μm-thick silvered poly(4-methyl-1-pentene) (PMP) sheet (Figure S7), first demonstrated as a radiative cooler by Grenier,[35] was chosen as the selective emitter, and a 127-μm-thick silvered poly(vinylidene difluoride) (PVdF) sheet (Figure S7) was chosen as the broadband emitter. The setup in Figure 3A was exposed to the environment, either at night or facing away from direct sunlight to avoid the compounding effects of different R_{solar} of the samples. Details about the experiments are presented in Note S4. Notably, the samples were completely exposed to the air, making convective effects significant.

Experiment I, which conclusively demonstrates the thermoregulation effect, was performed at night (T_{amb} ~11°C, TPW 11.5 mm, windspeed 0–1 m s^{-1}) in Los Angeles, on a roof that had radiatively cooled to sub-ambient temperatures (by ~5°C) at night and also had a mildly warm pool (by ~11°C), allowing us to mimic both mild winter and mild summer conditions (Figure 3A). Initially, the samples were placed above the cold ground to represent mild winter conditions, and as shown in Figure 3B, the selectively emissive PMP sample was 0.21°C warmer than the broadband-emissive PVdF over an ~½ h period. The samples were then moved

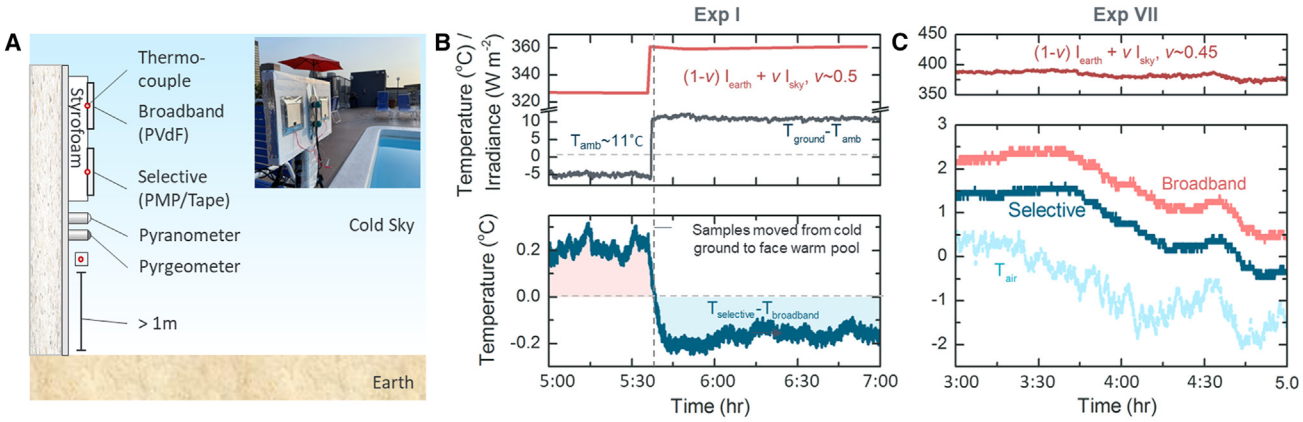

Figure 3. Proof-of-concept demonstration of the passive thermoregulation by selective LWIR emitters under partially controlled conditions

(A) Experimental setup.

(B) Experiment I. (Top) Pyrgeometric thermal irradiance measured along the horizontal direction and T_{ground} relative to T_{amb} (11°C). (Bottom) The PMP selective emitter was 0.21°C warmer than the PVdF broadband emitter when facing the cold ground mimicking mild winter conditions and became 0.16°C cooler when facing the warm pool mimicking mild summer conditions, conclusively showing the thermoregulation effect.

(C) Experiment VII, performed at night with the samples facing a ground simulator mimicking hot summertime terrestrial conditions. (Top) Pyrgeometric thermal irradiance measured along the horizontal direction. (Bottom) The T_{amb} and temperatures of the broadband and selective emitters, the latter being 0.86°C cooler. The experiments are detailed in Note S4 and Table S2 and compared with the theory in Figure 4C.

to face the warm pool to mimic the mild summer environment (the configuration shown in the inset of Figure 3A), causing the thermal irradiance on the samples to jump by 34 W m^{-2} from the terrestrial contribution (Figure 3B, top). Immediately, the relative temperature dropped, steadying with the PMP becoming ~0.15°C cooler than the PVdF over an ~$1^1/_4$ h period, conclusively showing the thermoregulatory potential of selective LWIR emitters (Figure 3B; Table S2). Experiment II, done with the setup facing the warm pool mimicking mild summer conditions over an extended 8 h period (T_{amb} ~17.5°C, TPW 28 mm, windspeed 0–1 m s^{-1}), showed an average relative cooling of 0.26°C by the PMP (Table S2). To represent a scenario with a hotter ground, experiment VII was done with the PVdF emitter and a selective emitter made from Scotch tape (Figure S27) placed in front of a ground simulator mimicking a summertime ground ~38°C hotter than T_{amb} (Figure 3C; Table S2). For the given meteorological conditions (T_{amb} ~0°C, TPW 5 mm, windspeed <0.5 m s^{-1}), the selective emitter was found to be ~0.86°C cooler than the broadband emitter over a 2 h period.

We also performed further experiments in summer and winter weather conditions. Experiment III was performed during a summer day on a parking lot (Note S4). There, under exposure to a hot environment (T_{ground} ~57°C, T_{amb} ~31.6°C, TPW 31 mm, windspeed 0.5–2 m s^{-1}), the PMP selective emitter was 0.43°C cooler than the PVdF (Figure 4A), even under considerable winds, and despite the PMP absorbing ~4 W m^{-2} more of the downwelling diffuse and terrestrially reflected sunlight. Experiment IV, which was done on a summer day on a roof in even windier conditions (T_{ground} ~55°C, T_{amb} ~21°C, TPW 15 mm, windspeed 1–3 m s^{-1}), showed relative cooling of 0.47°C by the PMP selective emitter (Figure 4C), including periods when cooling was as much as ~0.75°C under calmer winds (Note S4). Experiment V, which was done under mild winter conditions (T_{ground} ~11.5°C, T_{amb} ~15°C, TPW 17 mm, windspeed 0–1 m s^{-1}) on a rooftop, showed a very slight relative warming by the PMP (~0.02°C). Experiment VI, which was performed in colder and more representative winter conditions (T_{ground} ~2.4°C, T_{amb} ~7°C, TPW 7.5 mm, windspeed 0–0.5 m s^{-1}), showed a relative warming of 0.13°C by the PMP (Figure 4B).

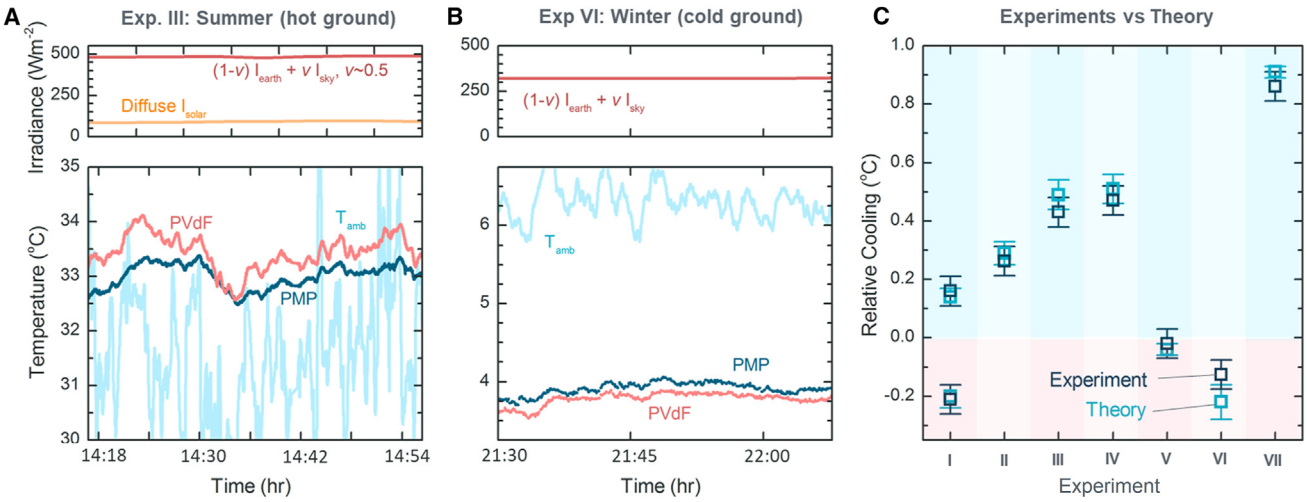

Figure 4. Additional summertime and wintertime steady-state temperature experiments

(A) Experiment III representing summertime conditions. (Top) Pyrgeometric thermal irradiance and solar irradiance measured along the horizontal direction. (Bottom) As expected, the PMP selective emitter is ~0.43°C cooler than the PVdF broadband emitter despite convective effects and greater solar heating.

(B) Experiment VI representing wintertime conditions. (Top) Pyrgeometric thermal irradiance measured along the horizontal direction. (Bottom) As expected, the PMP selective emitter is ~0.13°C warmer than the PVdF broadband emitter.

(C) Results of all the experiments compared against the theoretical predictions. As evident, the set of seven measurements is consistent with and validates the theory. Error bars represent the uncertainties in the experimental and theoretical results. Details of the theoretical predictions are presented in Note S4. All experiments are detailed in Table S2.

Accounting for uncertainties in the modeling and experimental measurements (Note S4), the eight experimental measurements presented here are all consistent with the theoretical predictions (Figure 4C). Given that consistency is observed across different seasons and locations characterized by different T_{ground}, T_{amb}, TPW, and windspeeds, we believe that the results conclusively validate the radiative thermoregulation capability of the selective LWIR emitters that we propose.

It should be noted that the differences in steady-state temperatures observed can seem deceptively modest. This is, in small part, due to the fact that PMP and PVdF are non-ideal selective and broadband emitters, respectively, and as used were off-the-shelf materials not optimized for performance. But the results have more to do with the nature of the experiment and should not be conflated with the performance of radiative coolers on buildings, which have an indoor environment and large thermal inertias (Note S5), unlike the setup in Figure 3A or previous demonstrations in the literature.[6,11,19] It is also important to distinguish *relative* cooling/heating of vertically oriented emitters (which can be low even for sky-facing designs[36]) from the *absolute* sub-ambient cooling by sky-facing emitters (which are often aided by convection shields, unlike our designs).[6,11,19] The purpose of experiments I–VI was to verify the theory, and in doing so, they confirm that selective and broadband emitters experience a large difference in heat flows through them (Figure 2; Note S6), which we demonstrate below.

Measuring differential power flows

To experimentally demonstrate that the observed temperature differences in Figure 4C indicate substantial differences in heat flow, we measured heat flows through broadband and selective emitters exposed to hot and cold ground conditions. For the hot ground experiment, a Scotch tape selective emitter (Figure S27) and the PVdF broadband emitter, both previously cooled to sub-ambient temperatures,

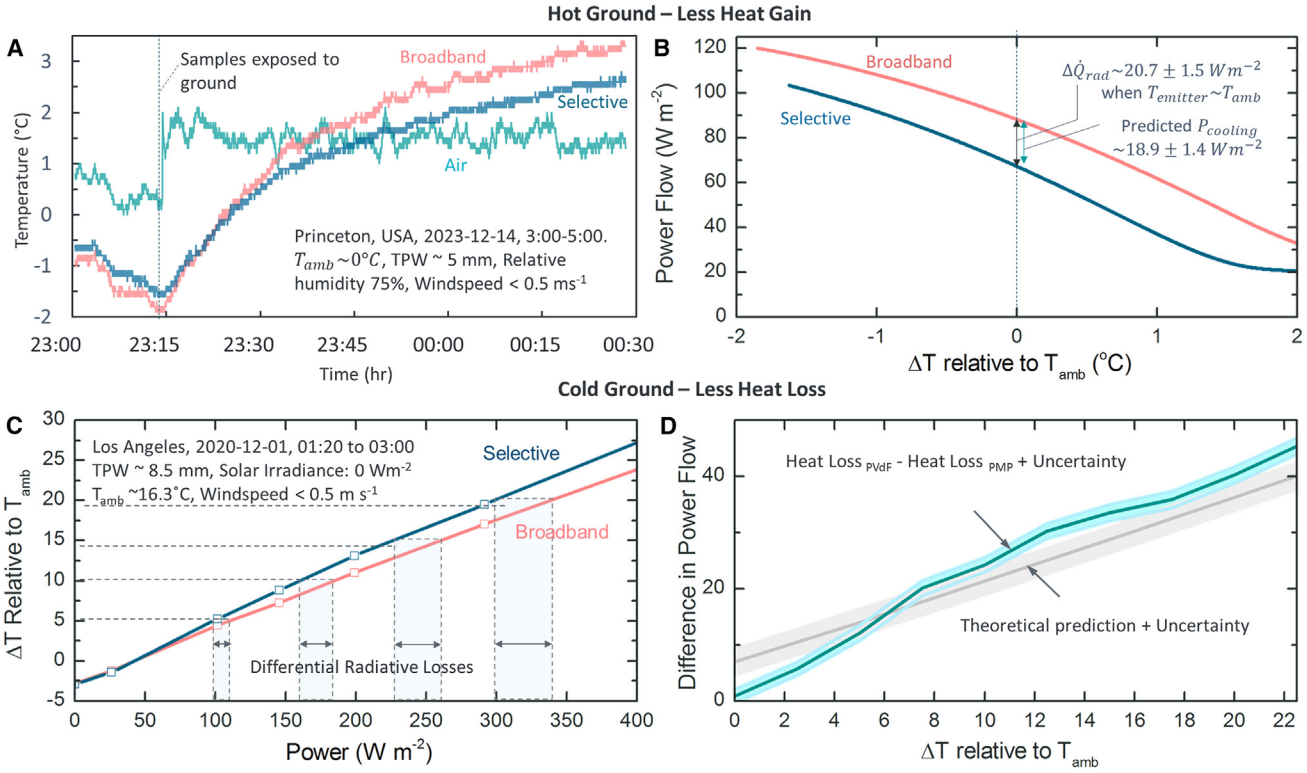

Figure 5. Experiments demonstrating the significant differential heat flows through the selectively LWIR-emissive PMP and broadband-emissive PVdF emitters

(A) When exposed to a hot ground simulator, a broadband emitter gains heat at a faster rate than a selective LWIR emitter.

(B) Based on smooth mathematical fits of the temperature profile, the radiative heat gains of the two emitters were calculated as a function of $\Delta T = T_{emitter} - T_{amb}$, showing a theoretically consistent difference in cooling potential of 20.7 ± 1.5 W m^{-2}.

(C) Under cold conditions, a selective PMP emitter exhibited warmer temperatures than a broadband PVdF emitter when subjected to the same heat flow. Shaded areas show that at the same temperatures relative to T_{amb}, the PVdF has greater radiative heat loss than the PMP, as expected in the winter.

(D) The differential radiative heat losses of selective PMP and broadband PVdF emitters. The PMP has a lower heat loss, e.g., by ~12 W m^{-2} when 5°C warmer than T_{amb} and by ~33.5 W m^{-2} when 15°C warmer. Accounting for experimental uncertainties, and the complex environment, the results are consistent with the theory. Further details are provided in Note S4 and Figures S11 and S12.

were vertically exposed to and radiatively heated by a warm ground simulator 38°C above T_{amb} (Figures 5A and S12). It was observed that when at the same temperature relative to the environment, the selective emitter gained heat at a considerably slower rate than the broadband emitter (Figure 5A). Derivations of radiative heat gain at T_{amb} (i.e., $P_{cooling}$) showed that the selective emitter had an ~20.7 ± 1.5 W m^{-2} lower radiative heat gain (Figure 5B), consistent with a theoretical prediction of 18.9 ± 1.4 W m^{-2} for the meteorological conditions (T_{amb} ~0°C, T_{ground} ~38°C, TPW ~5 mm, windspeed <0.5 m s^{-1}). This ~20 W m^{-2} relative radiative cooling was seen across the range of near-ambient temperatures of the emitters.

For the cold ground experiment, we heated the PMP and PVdF samples at different rates under vertical exposure to the outdoor environment during a winter night in Los Angeles. As shown, the selectively LWIR-emissive PMP stays warmer than the broadband-emissive PVdF when heated at the same rate (Figure 5C) or, conversely, has a lower heat outflow for a given temperature (Figure 5D). The differences in heat outflow, e.g., ~12 and 33.5 W m^{-2} when both emitters are respectively 5°C and 15°C warmer than the cold air (which was still throughout the duration of the experiment), are radiative and significantly large. More importantly, they are close to theoretical

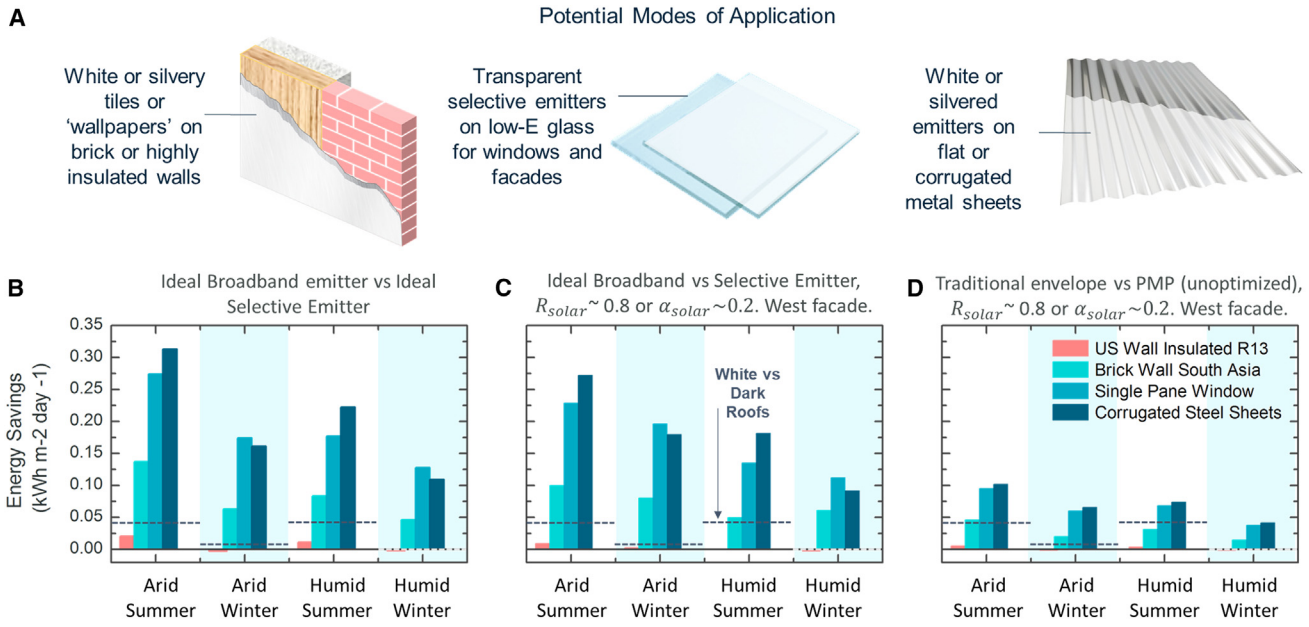

Figure 6. Potential modes of application of selective emitters and calculated energy savings

(A) Potential ways in which selective LWIR emitters could be applied onto vertical facades made from different materials.

(B) Peak summer and wintertime energy savings enabled by an ideal selective LWIR emitter over an ideal broadband emitter in arid and very humid locations for the different modes in (A).

(C and D) Analogous case for ideal selective LWIR and broadband emitters with R_{solar} ~0.8 (or for transparent designs α_{solar} ~0.2) on a west-facing facade (C) and LWIR-emissive PMP (Figure 7A) versus typical building envelopes ($\epsilon_{broadband}$ ~0.9) on a west facing facade, assuming R_{solar} ~0.88 or α_{solar} ~0.12 for both (D). Details of the model are provided in Notes S6 and S7, Figures S14–S19, and Tables S3–S5. Note: while the arid cases had typical atmospheric TPW levels (10.5 mm), the tropical TPW was exceptionally high (58.6 mm), especially for winter (Figure S23). Typical savings in the tropics may thus be higher, particularly in the winter. The dotted lines, which indicate savings for white roofs on single-family houses during peak summer and winter, are derived from data for Phoenix (desert) and Miami (tropical) in a work by Baniassadi et al.[38]

predictions (Figure 5D;Notes S3 and S4) and substantiate the large difference in heat flows predicted by our model. Promisingly, the large power flow differentials also hint at the achievable building energy savings, since, like the samples in Figure 5D, building facades can be 3°C–20°C warmer than T_{amb} in the winter (Figure 1A; Note S5). In the next section, we look at this in detail.

Implications for buildings—Energy savings model

The thermoregulatory capability of LWIR emitters on vertical building facades can yield significant energy savings. The precise amount depends on factors like geographic location, landscape (e.g., urban versus rural), and seasonal and diurnal variations of the atmospheric and terrestrial *spectral* irradiances. Here, as the first effort of its type, we integrate our spectral model (Figure 2) with a previously validated heat-transfer model developed by Anand and Sailor[37] to estimate raw building energy savings (Note S6). Our model assumes a constant indoor temperature of 25°C and a diurnally and seasonally varying outdoor environment, separated by different vertical walls/windows. Bearing in mind scenarios in both developing and developed countries, we chose four globally prevalent facade types—wooden walls with R13 insulation (which is recommended in most US climate zones), brick walls (common in South and South-East Asia), single-pane glass (the most common transparent facade), and corrugated metal sheets (used in resource-poor settings) (Figure 6A). As locations, we chose the arid southwestern United States (TPW ~10.5 mm) and a subtropical South Asian region that experiences exceptionally humid spells (TPW ~58.6 mm). Further details are provided in Note S6.

Our model shows that during peak summer in locations representing dry to extremely humid conditions, the ideal selective LWIR emitter can reduce building heat inflows by ~0.01–0.13 kWh m^{-2} day^{-1} for walls, depending on the insulation; ~0.18–0.27 kWh m^{-2} day^{-1} for windows; and ~0.23–0.32 kWh m^{-2} day^{-1} for metal sheets (Figure 6B). During winter, the ideal selective LWIR emitter can reduce heat outflow by ~0–0.06 kWh m^{-2} day^{-1} for walls, ~0.13–0.17 kWh m^{-2} day^{-1} for windows, and ~0.11–0.16 kWh m^{-2} day^{-1} for metal sheets (Figure 6B). We note here that the savings for windows are an underestimate, as glass windows have a lower broadband emittance than we assumed.[39] To put these values into context, the dotted lines in Figures 6B–6D represent energy savings per unit area when dark roofs of residential buildings are painted white in similar arid (Phoenix) and humid (Miami) locations and correspond to ~175 kg/year reduction in CO_2 emissions and ~US$56/year savings for an ~110 m^2 roof.[38] On a per-unit-area basis, the energy savings we show are comparable or several times larger. If one also accounts for the fact that buildings have wall-to-roof area ratios of ~2–10, then, assuming typical roof sizes (~100–1,000 m^2), it can be conservatively estimated that for small to moderately large buildings, our approach could reduce CO_2 emissions by ~0.1–5 tons/year and save ~US$50–1,000/year. In resource-poor settings that lack HVAC controls and high insulation, the thermoregulation effect may lead to more habitable living environments by reducing temperature fluctuations and reduce health risks arising from extreme weather.

While the results in Figure 6B represent the raw energy savings for ideal selective and broadband cases, Figure 6C shows the savings when west-facing facades that see the greatest heating loads are modestly solar reflective (R_{solar} ~0.8) or, for transparent facades, tinted (solar absorptance α_{solar} ~0.2). While the summertime savings for such modestly solar-reflective west-facing facades are lower than in Figure 6B, they nonetheless remain high for brick, glass, and metal facades, while the wintertime savings fall slightly or rise depending on the climate. However, the overall decrease in thermoregulatory benefit is small. In fact, for low-insulated facades like brick walls and windows, which constitute most global building facades, R_{solar} can be considerably lower than 0.5 before the thermoregulatory benefits disappear (Note S7). For facades that have lower solar heating loads—e.g., north- and south-facing facades in low-to moderate latitudes—the thermoregulatory benefits would be even greater and robust under sunlight. Indeed, the leeway on R_{solar} could allow the use of solar-infrared-reflective and/or fluorescent "cool colors" or dark-tinted glass, an intriguing possibility in terms of esthetics.[40–44] It should be noted, however, that using too dark a surface is inadvisable, as the combination of high solar absorptance and direct strong sunlight during part of the day can make the facade hotter than the ambient environment. At those times, a selective emitter would cool at a lower rate than a broadband one.

To show energy savings that may be immediately achievable, we compare the unoptimized, off-the-shelf PMP selective emitter we used in our experiment (Figures 3A and 7A) against typical building facades like white paint ($\epsilon_{Broadband}$ ~0.9). Both the PMP and the traditional facade are assumed to have R_{solar} ~0.88, like the most reflective commercial paints,[29] or for transparent facades, α_{solar} ~0.12. As shown, even in the unoptimized form, the PMP still achieves considerable summer and wintertime savings for facades with low insulation, which can lead to cost and CO_2 emissions reductions comparable to or greater than painting roofs white (Figure 6D) and which, given the availability of PMP and materials like PP (Figure 7A), could be realized in the near future.

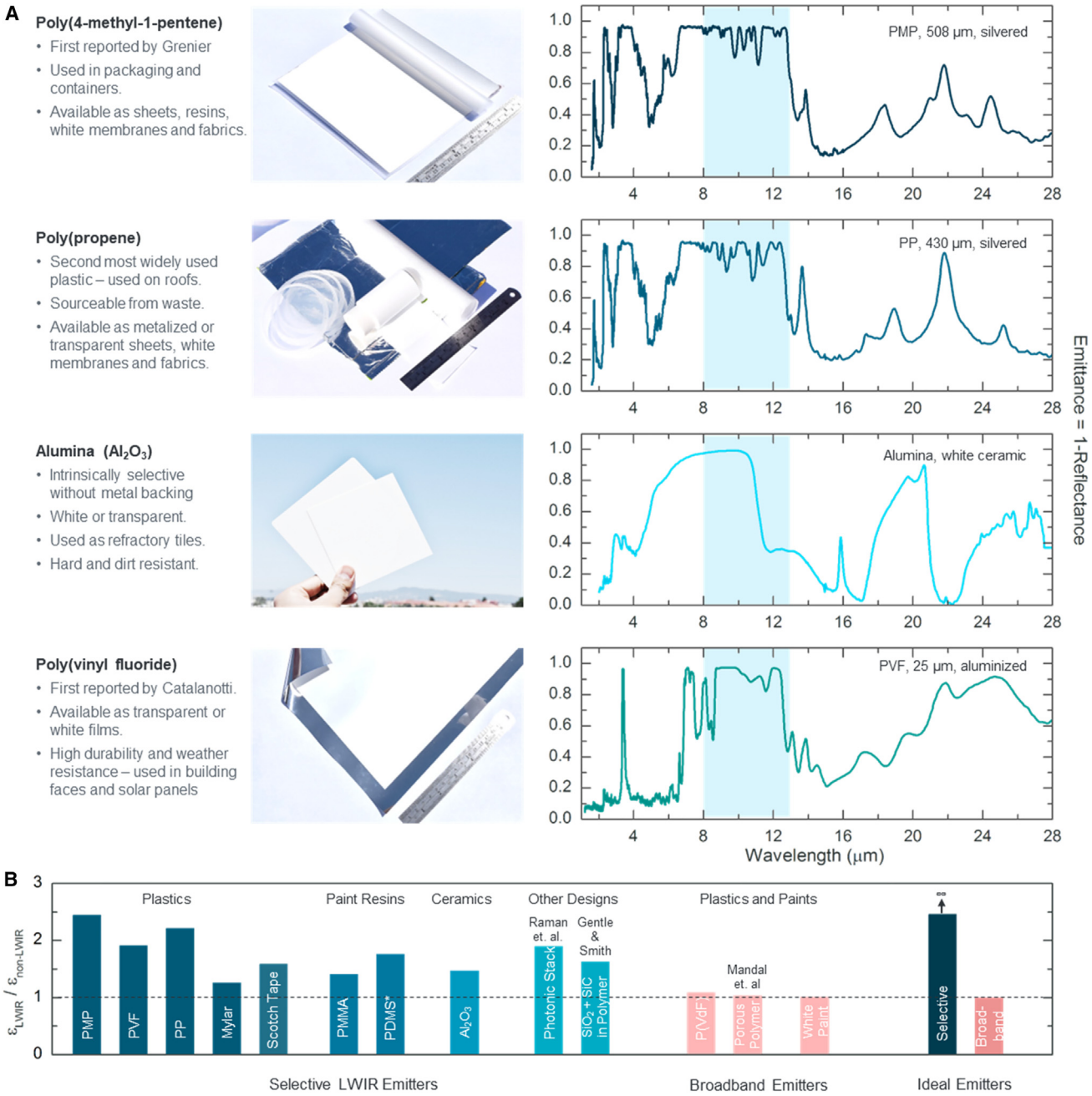

Figure 7. Selective LWIR emitters for thermoregulation of vertical facades can be realized in different forms

(A) Common examples include poly(4-methyl-1-pentene), poly(propene), alumina, and poly(vinyl fluoride) and are available in white, silvery, and transparent forms as shown in the pictures. Further examples are provided in Notes S10 and S11 and Figures S24–S28.

(B) The LWIR selectivity of different materials, characterized using the figure of merit $\eta = \epsilon_{LWIR}/\epsilon_{non\ LWIR}$ (Note S1). Note that the values of η we demonstrate are for materials obtained off the shelf and could be higher if optimized for optical thickness. *Calculation from experimentally derived complex refractive index.

Crucially, the energy savings we calculate here are *untapped and complementary rather than an alternative* to those of current solar reflection-based methods for walls and windows. Given that our approach is intended for vertical facades, it is a natural complement to previously reported super-white roof coatings and other sky-facing radiative coolers.[6,13,19,29] For walls, it can be the extension of white and colored cool

walls[45–47] that retains the benefits of solar reflectance while enabling radiative thermoregulation (Note S8). If made visibly transparent, selective emitters could also be used on windows and steel-and-glass architectures (Note S8). The variety of facades and the two weather extremes we model in Figures 6B–6D show the tremendous global promise of selective LWIR emitters on vertical building facades in terms of energy savings and thermal comfort.

LWIR-emissive materials for radiative thermoregulation

The building-level energy savings implications of the novel radiative thermoregulation effect we elucidated further motivated us to explore selective LWIR emitters for use on vertical facades. Given the intense and current global need for building thermoregulation, particularly in resource-poor settings, our focus was not on material innovation, but rather on previously known or unexplored selective LWIR emitters that could foreseeably be scaled and deployed on buildings in the near future. Accordingly, we investigated a range of selective LWIR emitters, including plastics, polymer resins, and ceramics, for potential use on buildings.

Figures 7A, S24, S25, and S27 show some examples, which are either made from common materials or already commercially available. Of these, PMP (more commonly known as TPX) was first demonstrated as a radiative cooler by Grenier in 1979,[35] while poly(vinyl fluoride) (PVF) was demonstrated by Catalanotti et al. in 1974.[48] Based on our prior work,[12] and prior[14] and subsequent[49] reports, we also note that thin films of common paint resins based on poly(methyl methacrylate) (PMMA) and poly(dimethylsiloxane)/silicone (PDMS) exhibit selective LWIR emittances (Figure S24), as do commercial films, like Scotch tape, that contain these materials and can be readily metallized (Figure S27). We also show, for the first time to our knowledge, metallized PP, biaxially oriented poly(ethene terephthalate) (BoPET, commonly known as Mylar), and alumina (Al_2O_3) ceramic tiles as selective emitters. The last of these combines shortwave Mie scattering and far-infrared Reststrahlen reflectance in a novel way to achieve a simultaneous R_{solar} and selective ε_{LWIR} without using metal.[50]

Figure 7B shows the selectivity (quantified as $\eta = \varepsilon_{LWIR}/\varepsilon_{non-LWIR}$) of commercially available variants of these materials derived from their emittance spectra (Notes S1 and S10). Despite being off the shelf and not optimized for optical properties, the selectivity of these materials ($\eta \gtrsim 1.3$) compares favorably with those of reported selective designs in the literature[34]—suggesting their immediate suitability and potential for further optimization from an optical standpoint. In particular, PP's combination of high ε_{LWIR} and η, even when unoptimized, is exceptional[34] and, given its ubiquity, represents a major material insight.

The materials we propose are perhaps some of the most scalable selective emitters currently available, as indicated by the conveniently created or acquired samples ($^1/_4$ to 1 ft^2 large) in Figure 7A. PMP and PVF are already produced at scale, with the latter made in metallized forms for building facades.[19,51–53] PMMA- and PDMS-based paint resins are well known for their long-standing use on building facades and could have an immediate impact on buildings. Among the new materials we show as selective emitters, PP and poly(ethene terephthalate) (PET) are the second and sixth most widely used plastics in the world,[54] produced in their metallized forms at $>10^8$ m^2 scales per year,[55] and sufficiently common to be sourced from plastic waste.[54] The spectrum for PP in Figure 7A was obtained from a discarded food container, which opens an intriguing possibility of extending lives of discarded

plastics by repurposing them into building envelopes. Aluminum oxide is a commonly used ceramic[56] and can be formed into commercially available tiles suitable for radiative cooling using conventional techniques (Figure 7A). Notably, some of these materials have long been established as radiative coolers[35,48,57] and recently used as components in large-scale broadband-emissive designs.[6,12,13,19,29] Further discussions about their scalability, and cost relative to exterior paints, are included in Note S10.

In terms of applicability and esthetics, it is noteworthy that the proposed materials can come in silvered, white, and (in the case of alumina and transparent conductor-backed polymers) transparent variants (Figures 7, S24, and S25). These make the designs suitable for a wide range of building facades such as walls and windows (Note S8; Figures S20 and S21). For white or silvered designs on walls, possible modes of application include silver or white "wallpapers" (e.g., metallized PMP, PVF, PP, Mylar, and their white porous or polyethene-coated variants, Note S10; Figure S26) and white tiles (e.g., Al_2O_3 ceramics, Figure 7A). Metal facades, which are intrinsically broadband reflective, could have plastics like PVF laminated[58] or PDMS/PMMA painted onto them. It should be noted that, as they are, the materials we show have R_{solar} of 0.90–0.99 (Note S11). But since our approach accommodates a range of R_{solar} values ($\gtrsim$0.50 for directly and lower for diffusely sunlit surfaces) (Note S7), our designs could be colored with IR-transparent dyes and pigments to widen their esthetic appeal.[40] In specific cases where solar reflection from walls is an issue, retroreflective[45] or darker variants may be used (Note S8).

For transparent facades, potential designs include transparent polymers laminated or painted, or SiO_xN_y[15] (Figure S25) or Al_2O_3 vapor deposited, onto low-emittance (low-ε) glasses that contain IR-reflective metal or oxide films.[59,60] For Al_2O_3, which intrinsically reflects λ >13 μm (Figure S25) without the aid of metal, ordinary glass would suffice.[50] Another possibility is widely available semi-transparent metalized Mylar and PP films, variants of which are already in use as solar-reflecting window laminates.[55]

Collectively, the designs we present combine high scalability, low cost, and ready availability, with versatility of application and appearance. In addition, PP's high ε_{LWIR} and η, and the metal-free selective emittance of white Al_2O_3 tiles for walls and transparent Al_2O_3 for windows, represent important insights into known materials. Since our designs could be foreseeably applied on vertical building facades worldwide (Figures 6A and 7A), and enable major, untapped energy savings (Figures 6B–6D), they could significantly impact building design and associated materials industries[61,62] and particularly benefit resource-poor settings that do not use insulation. Furthermore, the thermoregulation capability of selective LWIR emitters could motivate future design and optimization of highly scalable LWIR emitters approaching near-ideal ε_{LWIR} and η.[34]

Outlook

In this work, we have outlined a previously unexplored phenomenon in which the differential transmittance of the atmosphere to skyward and terrestrial radiative heat flows and seasonal variations in the earth's environment allow selective LWIR emitters on vertical facades of buildings to achieve a novel radiative thermoregulation. Our work elucidates and verifies the phenomenon, shows that it can enable substantial and untapped energy savings, and shows a range of highly scalable LWIR emitters toward this goal. Thus, this work exemplifies how subtle radiative phenomena in

Table 1. Comparison between selective LWIR emitters and other designs for vertical surfaces; radiative cooling textiles are also included

	Selective LWIR emitters for radiative thermoregulation	Broadband-radiative coolers and envelopes[6,19,29]	Low-ε glasses	VO_2-based broadband thermochromic windows[28,64]	Radiative cooling textiles[25–27,65]
Optical design	selective ε_{LWIR} (and variable R_{solar})	broadband ε (and variable R_{solar})	visible (semi-) transparency (and solar absorption), and TIR reflectance	high ε above and low ε below a transition temperature T_{trans}	broadband TIR transmittance or absorptance or controllable direct exposure of skin
In warm weather	reduced broadband terrestrial heat gain	broadband terrestrial heat gain overwhelms radiative cooling	no access to LWIR atmospheric window α_{solar} and low ε leads to unwanted selective solar heating	$T > T_{trans}$, broadband terrestrial heat gain $T < T_{trans}$, heating due to α_{solar} and low ε; likelier because of high T_{trans} (~60°C)	broadband terrestrial heat gain
In cold weather	reduced broadband terrestrial heat loss	broadband terrestrial heat loss causes overcooling	negligible heat loss to earth and sky	reduced heat loss to earth and sky	broadband terrestrial heat loss causes overcooling
Modes	walls, windows, textiles	walls, windows	windows	windows	textiles
Appearance	versatile	versatile	tinted	yellow tinted	preferably white
Materials	common, commercially available, and sourceable from waste	common and commercially available	commercially available	VO_2 is costlier and unstable in air[66,67]	commercially available
Fabrication and scalability	currently produced at very large scale, $>10^8$ m^2/year	currently produced at very large scale for buildings worldwide	currently produced at very large scale for buildings high precision required	currently small scale, $<10^2$ cm^2 precision required for large optical switching	currently produced at commercial scale
Cost	low	low	high	high	N/A for buildings
Suitability for resource-poor settings	high	high	moderate	low	N/A

our environment can be harnessed to complement existing solar-reflectance-based strategies on buildings and opens up new avenues for designing selective emitters for thermal comfort and energy efficiency in buildings.

So far, we have compared our approach with traditionally used broadband-emissive building envelopes and radiative coolers. Table 1 shows additional comparisons with low-ε glasses and VO_x-based thermochromic designs. As stated in Note S9, unlike our approach, broadband reflectors like low-ε glasses cannot access the cold heat sink of outer space (Figure S22), making them less effective in most summertime sky and terrestrial conditions. Furthermore, the α_{solar} ($\gtrsim$0.15) and low ε can inadvertently turn low-ε glasses to heat sources in the summer,[63] although they are highly effective in the winter. This also applies to aluminum facades, which come the closest to being feasible broadband reflectors for walls. Our design also compares favorably with thermochromic window coatings,[28] whose susceptibility to broadband terrestrial heating when broadband emissive and selective solar absorption due to tinting when IR reflective are two major limitations on performance. Our approach is also fundamentally different, as it involves a static rather than adaptive emitter that optimizes heat flows in a dynamic environment—a subtler but practically simpler approach.

Perhaps the most important difference our approach brings is its simplicity and synergy with current possibilities in building design. The common materials and long-established industrial techniques that can yield selective emitters could be more readily implementable than high-end, precision-engineered, and often air-sensitive thermoregulators recently proposed in the literature (Table 1). Given that the world's

most acute building thermoregulation needs are in resource-poor settings where building insulation is uncommon, this simplicity can go a long way toward real-life impact and addressing issues of equity.[68,69] Furthermore, the thermoregulation capability of our approach effectively reduces the need for thick insulation in buildings—opening an intriguing possibility for reducing associated environmental impacts and space constraints. We also note that reflection of the earth's upwelling non-LWIR glow by selective emitters could cool urban canyons faster.

In addition to use on vertical facades of buildings, selective LWIR emitters could also be used on vehicles, a significant fraction of whose surfaces are vertical. Another promising use could be in radiative cooling textiles. As evident from the thermal environment around the human beings in Figures 1A and S29, textiles like broadband-emissive fabrics or IR-transparent polyethene (which exposes the broadband-emissive skin underneath) can result in a net heat gain (Figure S30), particularly in hot urban environments. In colder environments, the same designs would be susceptible to overcooling (Figures 1A and S30). This makes radiative thermoregulation with broadband designs virtually impossible (Note S12), a fact that has been largely overlooked.[25–27,65] Selectively LWIR-emissive textiles, which could potentially be created by metallizing commercial PP or PMP fabrics (Figures 7A and S31), offer a fundamental advance in this regard, with thermally reflective textiles being another option for wintertime environments. Another possibility is the integration of LWIR emitters with phase-change materials or fluidic designs,[23,24] which could amplify their thermoregulation potential. A last, intriguing possibility would be to design emitters that are both selectively LWIR emissive and directionally emissive toward the sky. This can lead to highly efficient cooling in particular, as non-LWIR heat gain from both the ground and the sky would be minimized, making it a potentially fruitful research direction.

Since Trombe's seminal study of radiative cooling,[70] subsequent works have primarily focused on LWIR heat loss through the atmosphere toward the sky. Our exploration of the role of differential atmospheric transmittance and seasonal terrestrial irradiance, and selective LWIR emitters, which can thermoregulate buildings as the environment changes around them, could have major impacts and applications beyond those of sky-facing radiative cooling designs. We hope that this work will spur further research in scalable selective LWIR emitters for thermal comfort and regulation in the built environment and beyond.

EXPERIMENTAL PROCEDURES

Resource availability

Lead contact

Requests for further information and resources and reagents should be directed to Jyotirmoy Mandal (jm3136@princeton.edu).

Materials availability

This study did not generate new unique reagents.

Data and code availability

Data relevant to this work are provided in the article or the supplemental information.

SUPPLEMENTAL INFORMATION

Supplemental information can be found online at https://doi.org/10.1016/j.xcrp.2024.102065.

ACKNOWLEDGMENTS

J.M. thanks Prof. David Sailor of Arizona State University for providing and elucidating the raw data for Baniassadi et al.[38]; Dr. Tiphaine Galy and Prof. Laurent Pilon of the University of California, Los Angeles, for their assistance with preliminary measurements; and Prof. Sir Keith Burnett, Prof. Adam Overvig, and Dr. Kamal Krishna Mandal for helpful discussions. J.M. was supported by Schmidt Science Fellows, in partnership with the Rhodes Trust. A.P.R. acknowledges support from the Alfred P. Sloan Foundation and by the National Science Foundation under grant ECCS-2146577. J.B. was supported by a National Science Foundation Graduate Research Fellowship under grants DGE-1650605 and DGE-2034835.

AUTHOR CONTRIBUTIONS

J.M. originated the concept and explored materials and optical mechanisms for selective LWIR emitters. A.P.R. supervised the study. J.M. and A.P.R. designed the experiments. J.M., S.M., and A.R. performed thermography, pyrgeometry, and image processing. J.B. prepared samples for experiments. J.M. and J.B. performed the outdoor experiments. J.M. performed the spectroscopy. J.A. and J.M. performed the building energy calculations. J.M., A.P.R., and S.M. wrote the manuscript.

DECLARATION OF INTERESTS

The concept detailed in this paper was first publicly disclosed on arXiv on June 21, 2020, and expanded in subsequent updates until May 7, 2021. A provisional patent application (WO/2021/087128) has been filed related to this article.

Received: January 20, 2024
Revised: April 17, 2024
Accepted: June 5, 2024
Published: June 27, 2024

REFERENCES

1. International Energy Agency. (2019). 2019 Global Status Report for Buildings and Construction: Towards a Zero-Emission, Efficient and Resilient Buildings and Construction Sector. (Global Alliance for Buildings and Construction). https://www.iea.org/reports/global-status-report-for-buildings-and-construction-2019.

2. Campbell, I., Kalanki, A., and Sachar, S. (2018). Solving the Global Cooling Challenge: How to Counter the Climate Threat from Room Air Conditioners. Rocky Mountain Institute. www.rmi.org/insight/solving_the_global_cooling_challenge.

3. Salamanca, F., Georgescu, M., Mahalov, A., Moustaoui, M., and Wang, M. (2014). Anthropogenic heating of the urban environment due to air conditioning. JGR. Atmospheres *119*, 5949–5965. https://doi.org/10.1002/2013JD021225.

4. Flanner, M.G. (2009). Integrating anthropogenic heat flux with global climate models. Geophys. Res. Lett. *36*. https://doi.org/10.1029/2008GL036465.

5. de Munck, C., Pigeon, G., Masson, V., Meunier, F., Bousquet, P., Tréméac, B., Merchat, M., Poeuf, P., and Marchadier, C. (2013). How much can air conditioning increase air temperatures for a city like Paris, France? Int. J. Climatol. *33*, 210–227. https://doi.org/10.1002/joc.3415.

6. Mandal, J., Fu, Y., Overvig, A.C., Jia, M., Sun, K., Shi, N.N., Zhou, H., Xiao, X., Yu, N., and Yang, Y. (2018). Hierarchically porous polymer coatings for highly efficient passive daytime radiative cooling. Science *362*, 315–319. https://doi.org/10.1126/science.aat9513.

7. Cool Roof Rating Council Rated Products Directory. https://coolroofs.org/directory.

8. Harrison, A.W., and Walton, M.R. (1978). Radiative cooling of TiO2 white paint. Sol. Energy *20*, 185–188. https://doi.org/10.1016/0038-092X(78)90195-0.

9. Orel, B., Gunde, M., and Krainer, A. (1993). Radiative cooling efficiency of white pigmented paints. Sol. Energy *50*, 477–482. https://doi.org/10.1016/0038-092X(93)90108-Z.

10. Leroy, A., Bhatia, B., Kelsall, C.C., Castillejo-Cuberos, A., Di Capua H, M., Zhao, L., Zhang, L., Guzman, A.M., and Wang, E.N. (2019). High-performance subambient radiative cooling enabled by optically selective and thermally insulating polyethylene aerogel. Sci. Adv. *5*, eaat9480. https://doi.org/10.1126/sciadv.aat9480.

11. Raman, A.P., Anoma, M.A., Zhu, L., Rephaeli, E., and Fan, S. (2014). Passive radiative cooling below ambient air temperature under direct sunlight. Nature *515*, 540–544. https://doi.org/10.1038/nature13883.

12. Yu, N., Mandal, J., Overvig, A., and Shi, N. (2016). Systems and Methods for Radiative Cooling and Heating. patent application publication WO/2016/205717. filed June 6, 2016, and published December 22, 2016.

13. Gentle, A.R., and Smith, G.B. (2015). A Subambient Open Roof Surface under the Mid-Summer Sun. Adv. Sci. *2*, 1500119. https://doi.org/10.1002/advs.201500119.

14. Srinivasan, A., Czapla, B., Mayo, J., and Narayanaswamy, A. (2016). Infrared dielectric function of polydimethylsiloxane and selective emission behavior. Appl. Phys. Lett. *109*, 061905. https://doi.org/10.1063/1.4961051.

15. Eriksson, T.S., Jiang, S.-J., and Granqvist, C.G. (1985). Surface coatings for radiative cooling applications: Silicon dioxide and silicon nitride made by reactive rf-sputtering. Sol. Energy Mater. *12*, 319–325. https://doi.org/10.1016/0165-1633(85)90001-2.

16. Granqvist, C.G. (1981). Radiative heating and cooling with spectrally selective surfaces. Appl.

Opt. *20*, 2606–2615. AO. https://doi.org/10.1364/AO.20.002606.

17. Granqvist, C.G., and Hjortsberg, A. (1981). Radiative cooling to low temperatures: General considerations and application to selectively emitting SiO films. J. Appl. Phys. *52*, 4205–4220. https://doi.org/10.1063/1.329270.

18. Gentle, A.R., and Smith, G.B. (2010). Radiative Heat Pumping from the Earth Using Surface Phonon Resonant Nanoparticles. Nano Lett. *10*, 373–379. https://doi.org/10.1021/nl903271d.

19. Zhai, Y., Ma, Y., David, S.N., Zhao, D., Lou, R., Tan, G., Yang, R., and Yin, X. (2017). Scalable-manufactured randomized glass-polymer hybrid metamaterial for daytime radiative cooling. Science *355*, 1062–1066. https://doi.org/10.1126/science.aai7899.

20. Atiganyanun, S., Plumley, J.B., Han, S.J., Hsu, K., Cytrynbaum, J., Peng, T.L., Han, S.M., and Han, S.E. (2018). Effective Radiative Cooling by Paint-Format Microsphere-Based Photonic Random Media. ACS Photonics *5*, 1181–1187. https://doi.org/10.1021/acsphotonics.7b01492.

21. Wojtysiak, C.S. (2001). Radiative Cooling Surface Coatings. patent application publication AU2002302177A1. filed June 3, 2002, and published December 16, 2002.

22. Ono, M., Chen, K., Li, W., and Fan, S. (2018). Self-adaptive radiative cooling based on phase change materials. Opt Express *26*, A777–A787. https://doi.org/10.1364/OE.26.00A777.

23. Karlessi, T., Santamouris, M., Synnefa, A., Assimakopoulos, D., Didaskalopoulos, P., and Apostolakis, K. (2011). Development and testing of PCM doped cool colored coatings to mitigate urban heat island and cool buildings. Build. Environ. *46*, 570–576. https://doi.org/10.1016/j.buildenv.2010.09.003.

24. Mandal, J., Jia, M., Overvig, A., Fu, Y., Che, E., Yu, N., and Yang, Y. (2019). Porous Polymers with Switchable Optical Transmittance for Optical and Thermal Regulation. Joule *3*, 3088–3099. https://doi.org/10.1016/j.joule.2019.09.016.

25. Cai, L., Song, A.Y., Li, W., Hsu, P.-C., Lin, D., Catrysse, P.B., Liu, Y., Peng, Y., Chen, J., Wang, H., et al. (2018). Spectrally Selective Nanocomposite Textile for Outdoor Personal Cooling. Adv. Mater. *30*, 1802152. https://doi.org/10.1002/adma.201802152.

26. Zhang, X.A., Yu, S., Xu, B., Li, M., Peng, Z., Wang, Y., Deng, S., Wu, X., Wu, Z., Ouyang, M., and Wang, Y. (2019). Dynamic gating of infrared radiation in a textile. Science *363*, 619–623. https://doi.org/10.1126/science.aau1217.

27. Zeng, S., Pian, S., Su, M., Wang, Z., Wu, M., Liu, X., Chen, M., Xiang, Y., Wu, J., Zhang, M., et al. (2021). Hierarchical-morphology metafabric for scalable passive daytime radiative cooling. Science *373*, 692–696. https://doi.org/10.1126/science.abi5484.

28. Wang, S., Jiang, T., Meng, Y., Yang, R., Tan, G., and Long, Y. (2021). Scalable thermochromic smart windows with passive radiative cooling regulation. Science *374*, 1501–1504. https://doi.org/10.1126/science.abg0291.

29. Mandal, J., Yang, Y., Yu, N., and Raman, A.P. (2020). Paints as a scalable and effective radiative cooling technology for buildings. Joule *4*, 1350–1356. https://doi.org/10.1016/j.joule.2020.04.010.

30. Taha, H. (1997). Urban climates and heat islands: albedo, evapotranspiration, and anthropogenic heat. Energy Build. *25*, 99–103. https://doi.org/10.1016/S0378-7788(96)00999-1.

31. Stathopoulou, M., Synnefa, A., Cartalis, C., Santamouris, M., Karlessi, T., and Akbari, H. (2009). A surface heat island study of Athens using high-resolution satellite imagery and measurements of the optical and thermal properties of commonly used building and paving materials. Int. J. Sustain. Energy *28*, 59–76. https://doi.org/10.1080/14786450802452753.

32. Baldridge, A.M., Hook, S.J., Grove, C.I., and Rivera, G. (2009). The ASTER spectral library version 2.0. Rem. Sens. Environ. *113*, 711–715. https://doi.org/10.1016/j.rse.2008.11.007.

33. Touloukian, Y.S., and DeWitt, D.P. (1971). Thermophysical Properties of Matter - The TPRC Data Series. Thermophysical and Electronic Properties Information Analysis Center. https://apps.dtic.mil/sti/citations/ADA951943.

34. Mandal, J. (2021). A Survey of Radiative Coolers in the Literature. Preprint at engrXiv. https://doi.org/10.31224/osf.io/nup6c.

35. Grenier, P. (1979). Réfrigération radiative. Effet de serre inverse. Rev. Phys. Appl. *14*, 87–90. https://doi.org/10.1051/rphysap:0197900140108700.

36. Huang, X., Mandal, J., and Raman, A.P. (2021). Do-it-yourself radiative cooler as a radiative cooling standard and cooling component for device design. JPE *12*, 012112. https://doi.org/10.1117/1.JPE.12.012112.

37. Anand, J., and Sailor, D.J. (2022). Role of pavement radiative and thermal properties in reducing excess heat in cities. Sol. Energy *242*, 413–423. https://doi.org/10.1016/j.solener.2021.10.056.

38. Baniassadi, A., Sailor, D.J., and Ban-Weiss, G.A. (2019). Potential energy and climate benefits of super-cool materials as a rooftop strategy. Urban Clim. *29*, 100495. https://doi.org/10.1016/j.uclim.2019.100495.

39. Zhu, L., Raman, A.P., and Fan, S. (2015). Radiative cooling of solar absorbers using a visibly transparent photonic crystal thermal blackbody. Proc. Natl. Acad. Sci. USA *112*, 12282–12287. https://doi.org/10.1073/pnas.1509453112.

40. Lozano, L.M., Hong, S., Huang, Y., Zandavi, H., El Aoud, Y.A., Tsurimaki, Y., Zhou, J., Xu, Y., Osgood, R.M., Chen, G., and Boriskina, S.V. (2019). Optical engineering of polymer materials and composites for simultaneous color and thermal management. Opt. Mater. Express *9*, 1990–2005. https://doi.org/10.1364/OME.9.001990.

41. Levinson, R., Berdahl, P., and Akbari, H. (2005). Solar spectral optical properties of pigments—Part II: survey of common colorants. Sol. Energy Mater. Sol. Cell. *89*, 351–389. https://doi.org/10.1016/j.solmat.2004.11.013.

42. Berdahl, P., Boocock, S.K., Chan, G.C.-Y., Chen, S.S., Levinson, R.M., and Zalich, M.A. (2018). High quantum yield of the Egyptian blue family of infrared phosphors (MCuSi4O10, M = Ca, Sr, Ba). J. Appl. Phys. *123*, 193103. https://doi.org/10.1063/1.5019808.

43. Berdahl, P., Chen, S.S., Destaillats, H., Kirchstetter, T.W., Levinson, R.M., and Zalich, M.A. (2016). Fluorescent cooling of objects exposed to sunlight – The ruby example. Sol. Energy Mater. Sol. Cell. *157*, 312–317. https://doi.org/10.1016/j.solmat.2016.05.058.

44. Chen, Y., Mandal, J., Li, W., Smith-Washington, A., Tsai, C.-C., Huang, W., Shrestha, S., Yu, N., Han, R.P.S., Cao, A., and Yang, Y. (2020). Colored and paintable bilayer coatings with high solar-infrared reflectance for efficient cooling. Sci. Adv. *6*, eaaz5413. https://doi.org/10.1126/sciadv.eaaz5413.

45. Levinson, R., Chen, S., Slack, J., Goudey, H., Harima, T., and Berdahl, P. (2020). Design, characterization, and fabrication of solar-retroreflective cool-wall materials. Sol. Energy Mater. Sol. Cell. *206*, 110117. https://doi.org/10.1016/j.solmat.2019.110117.

46. Rosado, P.J., and Levinson, R. (2019). Potential benefits of cool walls on residential and commercial buildings across California and the United States: Conserving energy, saving money, and reducing emission of greenhouse gases and air pollutants. Energy Build. *199*, 588–607. https://doi.org/10.1016/j.enbuild.2019.02.028.

47. Zhang, J., Mohegh, A., Li, Y., Levinson, R., and Ban-Weiss, G. (2018). Systematic Comparison of the Influence of Cool Wall versus Cool Roof Adoption on Urban Climate in the Los Angeles Basin. Environ. Sci. Technol. *52*, 11188–11197. https://doi.org/10.1021/acs.est.8b00732.

48. Catalanotti, S., Cuomo, V., Piro, G., Ruggi, D., Silvestrini, V., and Troise, G. (1975). The radiative cooling of selective surfaces. Sol. Energy *17*, 83–89. https://doi.org/10.1016/0038-092X(75)90062-6.

49. Aili, A., Wei, Z.Y., Chen, Y.Z., Zhao, D.L., Yang, R.G., and Yin, X.B. (2019). Selection of polymers with functional groups for daytime radiative cooling. Materials Today Physics *10*, 100127. https://doi.org/10.1016/j.mtphys.2019.100127.

50. Mandal, J. (2021). In search of the ideal radiative cooling material: the promise of porous ceramics. In Bulletin of the American Physical Society (American Physical Society).

51. Ebnesajjad, S. (2012). Polyvinyl Fluoride: Technology and Applications of PVF, 1st edition (William Andrew).

52. Mitsui Chemicals TPX™ | Business and Products | MITSUI CHEMICALS AMERICA, INC. https://us.mitsuichemicals.com/service/product/tpx.htm.

53. Cs Hyde TPX Polymethylpentene Film | Sold by the Lineal Foot. CS Hyde Company. https://catalog.cshyde.com/viewitems/films/tpx-polymethylpentene-film..

54. Geyer, R., Jambeck, J.R., and Law, K.L. (2017). Production, use, and fate of all plastics ever made. Sci. Adv. *3*, e1700782. https://doi.org/10.1126/sciadv.1700782.

55. Flex Films Flex Films || Metalized Films. https://www.flexfilm.com/metallised-films.php..

56. R.J. Brook, ed. (1991). Concise Encyclopedia of Advanced Ceramic Materials (Pergamon).

57. Santamouris, M., and Feng, J. (2018). Recent Progress in Daytime Radiative Cooling: Is It the Air Conditioner of the Future? Buildings *8*, 168. https://doi.org/10.3390/buildings8120168.

58. Metal Alliance DuPont™ Tedlar® PVF Film: Long-Lasting Protection for Architectural Metal Roofing and Wall Panels..

59. Hamberg, I., Hjortsberg, A., and Granqvist, C.G. (1982). High Quality Transparent Heat Reflectors Of Reactively Evaporated Indium Tin Oxide. In Optical Coatings for Energy Efficiency and Solar Applications (SPIE), pp. 31–36. https://doi.org/10.1117/12.933251.

60. Glass, V.A. The Science of Low-E Coatings. https://glassed.vitroglazings.com/topics/the-science-of-low-e-coatings.

61. (2019-2025). Grandview Research Cool Roof Market Size & Share | Industry Report (Grandview Research). https://www.grandviewresearch.com/industry-analysis/cool-roof-market.

62. BusinessWire (2020). Global Low-E Glass Market Report (2019 to 2024) - CAGR of 5.4% Expected during the Forecast Period - ResearchAndMarkets.Com. BusinessWire. https://www.businesswire.com/news/home/20200214005183/en/Global-Low-E-Glass-Market-Report-2019-2024.

63. Mandal, J., Wang, D., Overvig, A.C., Shi, N.N., Paley, D., Zangiabadi, A., Cheng, Q., Barmak, K., Yu, N., and Yang, Y. (2017). Scalable, "Dip-and-Dry" Fabrication of a Wide-Angle Plasmonic Selective Absorber for High-Efficiency Solar–Thermal Energy Conversion. Adv. Mater. *29*, 1702156. https://doi.org/10.1002/adma.201702156.

64. Batista, C., Ribeiro, R.M., and Teixeira, V. (2011). Synthesis and characterization of VO2-based thermochromic thin films for energy-efficient windows. Nanoscale Res. Lett. *6*, 301. https://doi.org/10.1186/1556-276X-6-301.

65. Zhu, B., Li, W., Zhang, Q., Li, D., Liu, X., Wang, Y., Xu, N., Wu, Z., Li, J., Li, X., et al. (2021). Subambient daytime radiative cooling textile based on nanoprocessed silk. Nat. Nanotechnol. *16*, 1342–1348. https://doi.org/10.1038/s41565-021-00987-0.

66. Chang, T., Cao, X., Li, N., Long, S., Zhu, Y., Huang, J., Luo, H., and Jin, P. (2019). Mitigating Deterioration of Vanadium Dioxide Thermochromic Films by Interfacial Encapsulation. Matter *1*, 734–744. https://doi.org/10.1016/j.matt.2019.04.004.

67. Cao, X., Chang, T., Shao, Z., Xu, F., Luo, H., and Jin, P. (2020). Challenges and Opportunities toward Real Application of VO2-Based Smart Glazing. Matter *2*, 862–881. https://doi.org/10.1016/j.matt.2020.02.009.

68. Mani, M., Bandyopadhyay, S., Chonabayashi, S., Markandya, A., and Mosier, T. (2018). South Asia's Hotspots : Impacts of Temperature and Precipitation Changes on Living Standards. (World Bank).

69. Royte, E. (2021). Too Hot to Live. Natl. Geogr. Mag. 40–65.

70. Trombe, F. (1967). Perspectives sur l'utilisation des rayonnements solaires et terrestres dans certaines régions du monde. Rev. Gen. Therm. *6*, 1215–1234.